Diagnostic ions guided 2D-locating strategy for characterization of chemical analogues in complex herbal medicines using liquid chromatography-ion mobility-mass spectrometry

Recommended Citation

Diagnostic ions guided 2D-locating strategy for characterization of chemical analogues in complex herbal medicines using liquid chromatography-ion mobility-mass spectrometry

Meng-Ning Li[1], Zi-Xuan Zhang[1], Hui-Ying Wang, Wen Gao, Ping Li, Hua Yang*

State Key Laboratory of Natural Medicines, China Pharmaceutical University, No. 24, Tongjia Xiang, Nanjing, 210009, China

Abstract

Rapid characterization of chemical analogues in potentially toxic complex matrix was essential for prevention of accidental poisoning. On the basis of the fragment ions possessed not only the same retention times (RT) but the same drift times (DT) on liquid chromatography-ion mobility-mass spectrometry (LC-IM-MS), an alternating frames (AF)-data independent acquisition (DIA) was utilized for simultaneous detection and rapid match of precursor/product ions with a fast switch of low/high collision energy (CE). A diagnostic ions guided 2D-locating strategy was developed for identification of chemical analogues in potentially toxic herbal medicines using LC-IM-MS. Firstly, the 2D-locations (RT, DT) of diagnostic ions were screened from high-fragment IM-MS frames according to their m/z. Then, the correlated precursor ions were extracted from the complex background interference in low-fragment IM-MS frames based on diagnostic ions' 2D-locations. Finally, the remained ions were characterized using double-bond equivalent analysis combined with MS/MS fragment interpretation. Totally, 236 diterpene alkaloids including eight compounds with potential new esterification types were characterized in processed lateral roots of *Aconitum carmichaelii* Debx. Moreover, the LC-IM-MS distribution regularities of diterpene alkaloids with various chemical structure types were further investigated and discussed. This study presented an innovative idea for revealing the chemical basis related to the toxicities of potentially poisonous herbal medicines to ensure the medication safety.

Keywords: Data independent acquisition, Diterpene alkaloids, Drift time, Liquid chromatography-ion mobility-mass spectrometry, Retention time

1. Introduction

Herbal medicines have been increasingly focused by the public and widely applied to prevention or treatment of various diseases around the world. However, some herbal materials were potentially toxic, which might cause severe adverse reactions, poisoning, and even death [1]. Rapid and effective risk assessment of potentially toxic complex samples was significant for human safety and health [2]. *Aconitum* L., a large genus of *Ranunculaceae* family containing more than 300 species, widely distributed in the north temperate zone including most of countries and territories in Asia [3], Europe [4], and North America [5]. Diterpene alkaloids were the dominant bioactive components in *Aconitum* species [6], which were reported to possess analgesic [7], anti-arrhythmic [8], and anti-inflammatory [9] activities. However, most of diterpene alkaloids in *Aconitum* species also have severe toxicities [10], leading to their narrow therapeutic ranges and high risks of poisoning [11]. In the last decades, cases of aconite poisoning frequently occurred due to unexpected overdose or intentional murder [12,13]. Thus, preliminary evaluation of the toxicities was essential to prevent accidental poisoning and ensure medication safety before external or internal

administration of complex matrixes derived from *Aconitum* herbs or unknown samples probably doped by diterpene alkaloids. The toxic levels of diterpene alkaloids mainly depended on their chemical skeletons and substructural groups, especially for the ester groups in their chemical structures [14]. Take C19-aconitine diterpene alkaloids as examples: the ester-types (e.g., aconitine and 14-*O*-benzoylaconine) had significantly higher toxicity than the aminol-type (e.g., aconine) diterpene alkaloids [15]. Therefore, characterization and differentiation of diterpene alkaloids by their structural types could provide primary evidence for toxicity assessment of *Aconitum* species. The major challenges for identification of diterpene alkaloids were the existence of numerous isomers or analogues at trace levels due to their various skeleton-types, abundant hydroxylation sites, and diverse esterification-types [16].

Recently, liquid chromatography (LC) tandem with high-resolution mass spectrometry (HRMS) has been widely applied to characterization of multiple components in various complex samples based on its integrated advantages of quick separation, high sensitivity, high resolution, and high mass accuracy [17]. For structural elucidation of compounds using tandem mass spectrometer, the selection of acquisition modes for MS/MS spectra was important [18]. Comparing with conventional data dependent acquisition (DDA), the data independent acquisition (DIA) modes were more applicable in principle for structural analysis of trace compounds based on their higher coverage of MS/MS information and wider precursor ions selection independent of ion intensity [19]. Nevertheless, the product ions in the MS/MS spectra were generated from the precursor ions of multiple co-eluted components during DIA, which were difficult to directly identify their chemical structures and needing further deconvolution based on another dimension of parameters [20]. Ion mobility (IM), an emerging hot technology for separation of co-eluted component ions based on their spatial structures, are increasingly utilized to analyze various complex matrixes with multiple components [21]. When the collision induced dissociation (CID) happened after IM-separation, the generated fragment ions could theoretically possess not only the same retention times (RT) but also the same drift times (DT) as their corresponding precursor ions [22]. Based on this principle, the interested components could be rapidly located according to the 2D-location (RT, DT) of their diagnostic fragment ions, which might benefit for screening of trace analogues in complex matrix. Single scheme (SS), the most common all ion

fragmentation-DIA mode, was operated through continuously activated CID for all precursor ions, which needing extra injection of MS full scan. Alternating frames (AF) was an IM-based all ion fragmentation-DIA mode operated through a fast-switch alternate acquisition of IM-frames with low and high collision energy (CE) [23]. This mode enabled simultaneous acquisition and discrimination of precursor ions and fragment ions within the same injection. The precursor ions existed in the low-fragment IM-frames, whereas fragment ions could be observed in the high-fragment IM-frames. Moreover, the product ions could directly correlate with their precursor ions by overlapping the low-fragment and high-fragment IM-frames at the same 2D-location (RT, DT).

In this study, diagnostic ions guided 2D-locating strategy was developed with AF-DIA modes on liquid chromatography-ion mobility-mass spectrometry (LC-IM-MS), including four detailed steps: Step 1: Investigation of analogues' fragment patterns and selection of diagnostic ions. Step 2: Screening of diagnostic ions based on their *m/z* and recording their 2D-locations (RT, DT) in high-fragment IM-frames. Step 3: Extraction of correlated precursor ions in low-fragment IM-frames based on the 2D-locations of diagnostic ions. Step 4: Characterization of analogues by double bond equivalents (DBEs) analysis and product ion/fragment pathway interpretation. This strategy was further applied for targeted screening and profiling of diterpene alkaloid analogues with diverse toxicities in processed lateral roots in *Aconitum carmichaelii* Debx. (Chinese: *Fu-Zi*, FZ). As far as was known, there were limited literatures reported the application of LC-IM-MS on analysis of small molecular analogues in herbal materials especially for traditional Chinese medicines. This study was expected to present an original method for revealing the profiles of material basis in potentially toxic herbal medicines to preliminarily estimate the risks.

2. Methods

2.1. Herbal materials, reference substances, and chemical reagents

Six batches of FZ, including four batches of *Hei-shun-pian* (Batch Nos: HSP19090304, HSP20200515, HSP20200531, and HSP20200525) and two batches of *Bai-fu-pian* (Batch Nos: BFP20200509 and BFP20200525) were collected or purchased from Sichuan Province of China. All the obtained herbal materials were morphologically authenticated by Professor Ping Li. These voucher specimens were

deposited in State Key Laboratory of Natural Medicines (China Pharmaceutical University, Nanjing, China).

Reference substances of aconine, mesaconine, hypaconine, karakoline, and napelline were employed from Push Bio-technology Co. Ltd (Chengdu, China). Songoramine was obtained from BioBioPha Biotechnology Co. Ltd (Kunming, China). Songorine, neoline, talatizamine, beiwutine, 14-O-benzoylaconine, 14-O-benzoylmesaconine and 14-O-benzoylhypaconine were purchased from Must Biotechnology Co. Ltd (Chengdu, China). Mesaconitine, hypaconitine and fuziline were ordered from National Institute for the Control of Pharmaceutical and Biological Products (Beijing, China). The purities of all the reference substances mentioned above were not less than 95.0% (HPLC).

The deionized water (18.2 MΩ cm) was prepared with a Milli-Q purification system (Millipore, Bedford, MA, USA). The HPLC-grade methanol and acetonitrile were purchased from Merck (Darmstadt, Germany). The HPLC-grade formic acid was ordered from ROE Scientific Inc. (Newark, DE, USA).

2.2. Preparation of solutions for herbal samples and reference substances

For each batch of FZ, 0.5 g powder (60 mesh) of FZ was accurately weighed in triplicate, mixed with 25 mL methanol, and extracted with ultrasonication for 0.5 h. The extracting solutions were cooled down and then centrifuged at 13,000 rpm for 10 min. Finally, the supernatant was stored in dark at −80 °C before injecting to the LC-IM-MS system.

For reference substance solutions, 1 mg of each reference substance mentioned above was accurately weighed and dissolved in methanol as stock solutions. The stock solution of each reference substances was also stored in dark at −80 °C and further diluted 20 to 50 times with methanol before injecting to the instrument (the Supplemental Content can be found here: https://www.jfda-online.com/cgi/viewcontent.cgi?filename=1&article=3372&context=journal&type=additional&preview_mode=1).

2.3. Instrument conditions and parameters

An Agilent 1290 Infinity II UHPLC (Agilent Corp., Santa Clara, CA, USA) system equipped with a high speed binary pump, a multisampler, a thermostatical column compartment, and a diode-array detector was employed for chromatographic separation. The multiple components were separated on a Zorbax Eclipse Plus C18 column (3.0 × 100 mm, 1.8 μm, Agilent Corp., Santa Clara, CA, USA). The autosampler was kept at 4 °C with the injection volume set at 5 μL. For the binary pump, mobile phase A was water containing 0.1% (v/v) formic acid while phase B was acetonitrile. The flow rate was set at 0.4 mL min⁻¹ with a gradient program listed as follows: 0−5 min, 5% B; 5−15 min, 5%−10% B; 15−30 min, 10%−20% B; 30−40 min, 20%−25% B; 40−55 min, 25%−50% B; 55−60 min, 50%−100% B; 60−65 min, 100% B. The posttime was set at 5 min for column equilibration between injections. For the thermostatical column compartment, the column temperature was kept as 30 °C during analysis.

The UHPLC system was connected with an Agilent 6560 ion mobility-quadrupole time-of-flight mass spectrometer (IM-QTOF MS, Agilent Corp., Santa Clara, CA, USA). The Dual Auto Jet Stream electrospray ionization (ESI) source was performed with positive ionization mode. The drying gas (N_2) temperature was set at 325 °C with flow rate as 10 L min⁻¹. The nebulizer was kept at 35 psig. The temperature and flow rate for sheath gas (N_2) were 350 °C and 11 L min⁻¹, respectively. The capillary voltage was 3500 V. The nozzle voltage was 1000 V. The fragmentor was 350 V.

Data acquisition was performed on IM-QTOF mode with an alternating frames (AF) mode. Under this type of mass spectra acquisition process, the precursor ions could be observed in the low-fragment IM-frames with no CID activated, whereas the fragment information were obtained in high-fragment IM-frames with fixed CE set at 45 eV. The mass ranges for acquisition of both low- and high-fragment IM-frames were m/z 40−1000. For IM-MS acquisition rate, the frame rate and the IM transient rate were 0.9 frames/s and 13 IM transients/frame, respectively. The drift time was limited not more than 80 ms. The TOF transient rate was automatically calculated as 489 transients/IM transients. For detection of more trace components, the fill time and release time of IM-trap funnel were set as 30,000 μs and 300 μs, respectively. The drift tube was operated with drift gas of high-pure nitrogen (purity ≥99.999%) maintained at a proper status (Pressure: 3.95 Torr; Temperature: 25 °C). A low uniform electric field was selected for better IM-separation of chromatographic co-eluted components with the entrance and exit voltage at 1000 V and 250 V (Drift tube length: 0.8 m; Drift tube uniform electric field intensity: 937.5 V/m). For other IM parameters of voltages for high-pressure funnel, both the delta voltage and the radio-frequency (RF) were set at 150 V. For the IM-trap, the delta voltage was 180 V, whereas the RF was set at 150 V. For the rear funnel,

the RF was set at 150 V. To obtain TOF mass and IM accuracy, mass calibration/check was operated with the Agilent ESI-Low concentration Tuning Mix (containing calibrant ions at m/z 118.0863, 322.0481, 622.0290, 922.0098, 1221.9906, 1521.9715, 1821.9523, 2121.9332, 2421.9140, and 2721.8948 at positive ion mode, Agilent Corp., Santa Clara, CA, USA). Data acquisition was performed by utilizing MassHunter Workstation Data Acquisiton Software version B.09.00 (Agilent Corp., Santa Clara, CA, USA).

2.4. Data analysis

Data evaluation was carried out on MassHunter Workstation Qualitative Analysis version B.09.00 (Agilent Corp., Santa Clara, CA, USA) and Mass-Hunter Workstation IM-Browser version B.08.00 (Agilent Corp., Santa Clara, CA, USA). For ions extraction, MassHunter Mass Profiler version B.08.01 (Agilent Corp., Santa Clara, CA, USA) were employed. The internal function "find features" was utilized for molecular features extraction of FZ samples. For detailed set up parameters, the ion intensity was limited as not less than 100, the isotope model was "Common organic molecules", and the charge states were limited as 1. For peak alignment, the tolerances of RT and DT were respectively set at ±0.3 min and ±1.5% with the mass errors were limited as ±(5.0 ppm + 5 mDa). The RT and DT ranges were limited as 2–65 min and 30–65 ms, respectively. For extraction of raw data in low-fragment IM-MS frames, the m/z ranges were not limited. For extraction of diagnostic ions in high-fragment IM-MS frames, the m/z ranges were set at 44.04–44.06, 58.05–58.07, 105.02–105.04, 131.04–131.06, 135.03–135.05 and 165.04–165.06 for locating the $[C_2H_6N]^+$, $[C_3H_8N]^+$, benzoyl $[C_7H_5O]^+$, cinnamoyl $[C_9H_7O]^+$, anisoyl $[C_8H_7O_2]^+$, and veratroyl $[C_9H_9O_3]^+$ residue ions, respectively.

3. Results

3.1. Comparison of DIA modes on LC-IM-MS

For detection of more comprehensive MS/MS fragment information, data independent acquisition (DIA) modes were selected for analysis of diterpene alkaloid analogues in FZ. There were two diverse DIA modes on LC-IM-MS: Single scheme (SS) and Alternating frames (AF). Generally, the information of molecular ions should be obtained using MS full scan mode (Fig. 1-A1, A2 & A3) before SS-DIA (Fig. 1-B1, B2 & B3). The sample injection and data acquisition should be operated at least twice for the same sample, which might be time-consuming and adverse to high throughput analysis. In addition, the researchers had to manually associate the precursor ions and fragment ions across at least two individual datafiles (MS full scan data and SS-DIA data). This might be labor-consuming and increase the probability of wrong correlation between precursor ions and product ions. During AF-DIA, the information of precursor ions and product ions could be simultaneously obtained within the same injection by a fast-switch alternated acquisition at low CE (Fig. 1-C1, C2 & C3) and high CE (Fig. 1-D1, D2 & D3), respectively. Furthermore, the correlation between precursor ions and product ions could be directly observed and established based on their drift times by overlapping the IM frames at the same retention time (Fig. 1-E1, E2 & E3). Therefore, the AF-DIA mode was selected.

3.2. Selection of diagnostic fragment ions for diterpene alkaloids

The obtained LC-IM-MS data were processed with the proposed diagnostic ion guided 2D-locating strategy for rapid characterization of diterpene alkaloid analogues in FZ samples. The schematic diagram was shown as Fig. 2. To the beginning, the fragmentation pathways of diterpene alkaloids were investigated based on MS/MS spectra of reference standards and previous literatures [24–28]. Based on the similar sub-groups existed in their chemical structures, common fragment ions could be generated and observed in the MS/MS spectra of several diterpene alkaloids. For most of C19-diterpene alkaloids and some C20-diterpene alkaloids (e.g., napellines), diagnostic amine residue ions at m/z 58.06 (Fig. 3-A1, B1 & C1) and m/z 44.05 (Fig. 3-D1, E1 & F1) could be detected in their MS/MS spectra, corresponding to existence of N-ethyl and N-methyl groups in their structures, respectively. In addition to amine residue ions, the ester-cleavage behaviors could only be observed in the ester-type diterpene alkaloids [24–28]. The ester-cleavage exhibited different appearance and have diverse basis for recognition of various esterification types. For conventional short-chain-lipo and long-chain-lipo esters, the ester-bond cleavage only exhibited as intact neutral losses of acids, such as $C_2H_4O_2$ (acetic acid, 60 Da, Fig. 3-E1) and $C_{18}H_{32}O_2$ (linoleic acid, 280 Da, Fig. 3-F1) [24–26]. The diterpene alkaloids with aromatic ester groups in their chemical structures usually possessed extremely larger toxicities than other compounds without these substructures in *Aconitum* species [29,30]. Due to the directly linkages between carbonyl group and large conjugated systems, the aromatic acyl residue
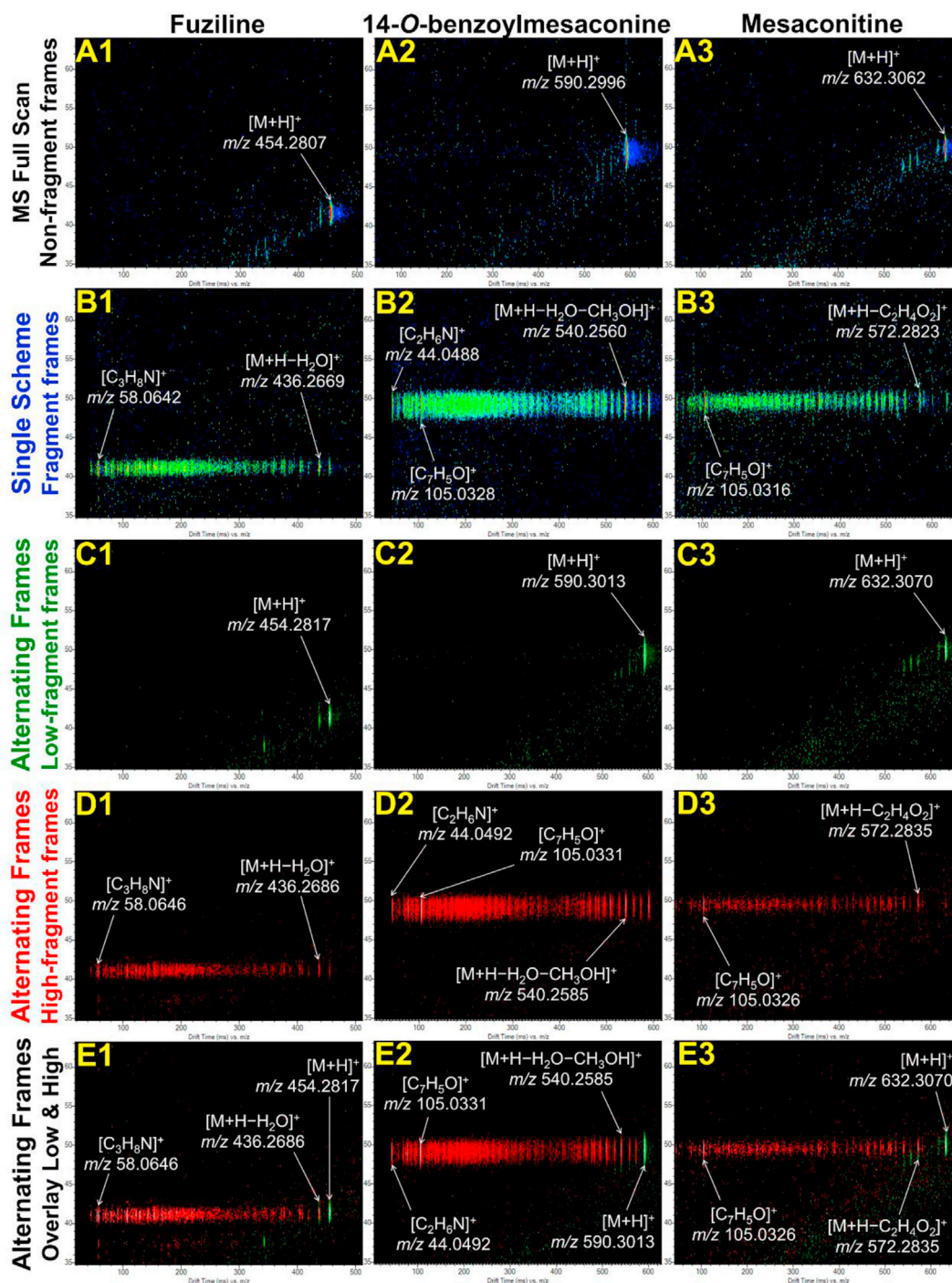
Fig. 1. Comparison of IM-frames in full scan (A1–A3), single scheme-DIA (B1–B3), and alternating frames-DIA (C1–C3, D1–D3, and E1–E3, corresponding to low-fragment, high-fragment, and overlapped IM-frames) modes with representative diterpene alkaloids (fuziline, 14-O-benzoyl-mesaconine, and mesaconitine) in FZ.

ions (e.g., m/z 105.03 and m/z 131.05, corresponding to benzoyl and cinnamoyl residue ions) could be obviously observed in their MS/MS spectra on ESI positive ionization mode (Fig. 3-C1, D1, E1 & F1) [27,28]. These ions were selected as diagnostic fragment ions for rapid identification of these highly

toxic ester-type diterpene alkaloids. The substructures and their potential corresponding diagnostic ions and neutral losses were listed in Table 1. The potential fragmentation pathways for generation of diagnostic ions or neutral losses above were interpreted in Fig. S1.
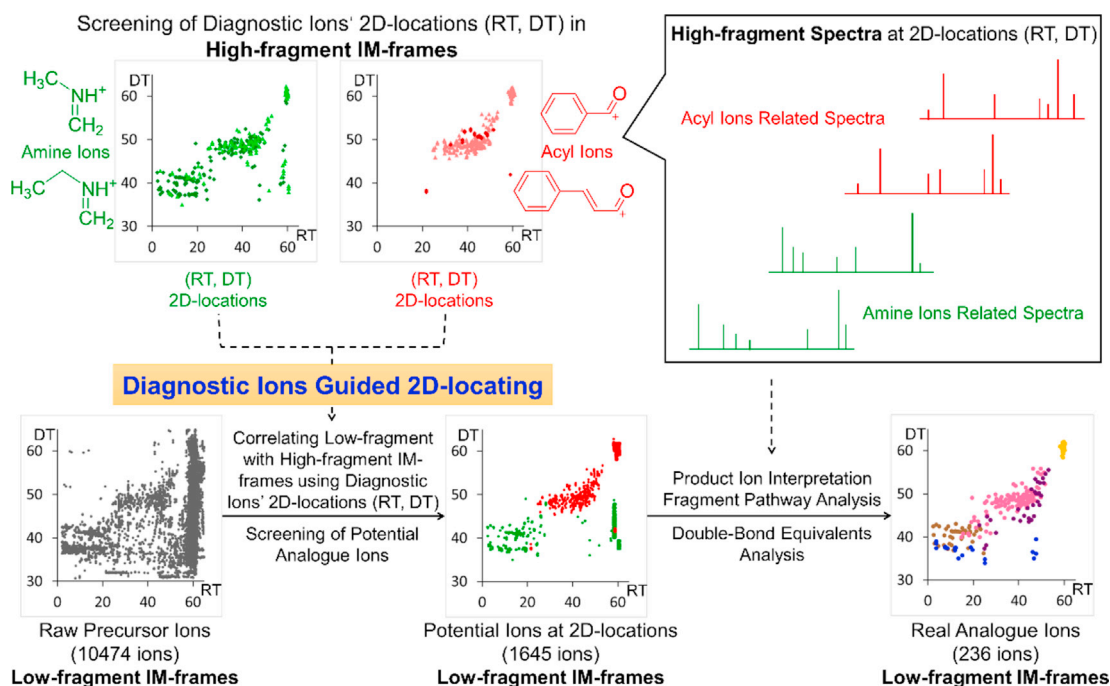
Fig. 2. Schematic diagram of diagnostic ion guided 2D-locating on LC-IM-MS.

3.3. Extraction of diterpene alkaloid precursor ions based on 2D-locations (RT, DT) of diagnostic ions

Totally, 10,474 precursor ions were preliminarily found in low fragment spectra of FZ samples (Fig. 4-A). Based on the principle of after-IM collision induced dissociation, the diterpene alkaloids' precursor ions should possess the same RTs and DTs as their fragment ions. Firstly, the diagnostic fragment ions listed in Table 1 were extracted from high-fragment IM-frames of FZ samples. Unfortunately, there were no anisoyl or veratroyl residue ions found in high fragment MS/MS spectra of FZ samples, representing no diterpene alkaloids with these two types of esterification were detected. These phenomena might be explained with the following two reasons. Comparing with benzoyl and cinnamoyl ions, the collision induced fragmentation (e.g.: cleavage of methoxyl groups on benzene rings) of anisoyl or veratroyl ions might more easily happen with the current LC-IM-MS parameters (especially for the relatively large collision energy at 45 eV). Secondly, the low content of these components might further decrease the intensities of anisoyl or veratroyl ions. In summary, 106, 208, 234, and 26 2D-locations of (RT, DT) belonged to $[C_2H_6N]^+$, $[C_3H_8N]^+$, benzoyl $[C_7H_5O]^+$, and cinnamoyl $[C_9H_7O]^+$ residue ions were extracted from high-fragment spectra of FZ (Fig. 4-B & C). Then, all the 2D-locations (RT, DT) of extracted diagnostic ion datapoints were recorded for further correlation with diterpene alkaloid precursor ions in low-fragment IM-frames. Based on the 2D-locations recorded, 1645 precursor ions were found in low-fragment IM-frames and correlated with the 2D-locations of diagnostic amine or acyl ions mentioned above. Among them, 843 precursor ions were associated with the acyl fragment ions, which might generate from highly toxic ester-type diterpene alkaloids (Fig. 4-D).

3.4. Characterization of diterpene alkaloids by double bond equivalents analysis combined with MS/MS fragmentation interpretation

The formulas of located precursor ions were calculated ($C \geq 19$, $H \geq 25$, $N = 1$, and $O \geq 1$) according to their m/z and charge states. Meanwhile, the double bond equivalents (DBEs) of these ions were automatically obtained. According to previous literatures [24−30], there were two conventional C19-diterpenoid skeletons (aconitanes and pyro-aconitanes) and four common types of C20-skeletons (napellines, hetisines, vakognavines, and atisines) in FZ. The chemical structures and DBEs of all detected skeletons and ester-substituents in FZ were exhibited in Fig. 5.

For further screening of target compounds in FZ, the DBE distribution for various type of diterpene alkaloids were investigated. To simplify the
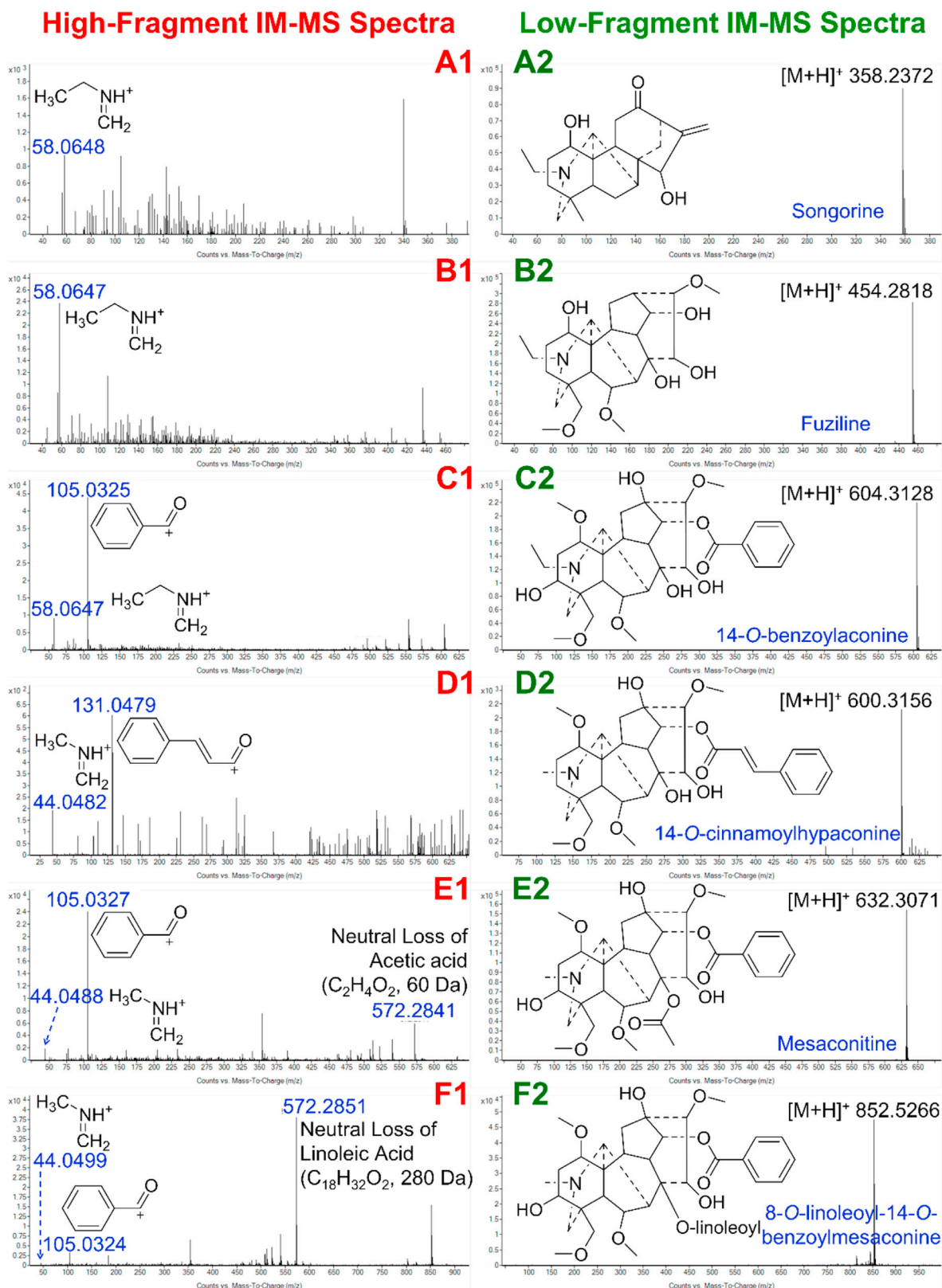
Fig. 3. High-fragment (left) and low-fragment (right) IM-MS spectra for representative diterpene alkaloids (A1 & A2: songorine; B1 & B2: fuziline; C1 & C2: 14-O-benzoylaconine; D1 & D2: 14-O-cinnamoylhypaconine; E1 & E2: mesaconitine; and F1 & F2: 8-O-linoleoyl-14-O-benzoylmesaconine) detected in FZ.

Table 1. Corresponding diagnostic fragment ions and/or neutral losses of potential substructures in diterpene alkaloids.

Contained Substructures	Residue Types	Diagnostic ions (m/z)	Neutral losses (Da)	Reference
N-methyl	Amine	$[C_2H_6N]^+$ (44.0495)	/	R.S.
N-ethyl	Amine	$[C_3H_8N]^+$ (58.0651)	/	R.S.
Acetoxyl	Simple ester	/	$C_2H_4O_2$ (60.0211)	R.S. & [24]
Propionyloxyl	Simple ester	/	$C_3H_6O_2$ (74.0368)	[25]
Isobutyryloxyl	Simple ester	/	$C_4H_8O_2$ (88.0524)	[25]
2-methylbutyryloxyl	Simple ester	/	$C_5H_{10}O_2$ (102.0681)	[25]
Myristoleoyloxyl	Lipo-ester	/	$C_{14}H_{26}O_2$ (226.1933)	[26]
Myristoyloxyl	Lipo-ester	/	$C_{14}H_{28}O_2$ (228.2089)	[26]
Palmitoleoyloxyl	Lipo-ester	/	$C_{16}H_{30}O_2$ (254.2246)	[26]
Palmitoyloxyl	Lipo-ester	/	$C_{16}H_{32}O_2$ (256.2402)	[26]
Linolenoyloxyl	Lipo-ester	/	$C_{18}H_{30}O_2$ (278.2246)	[26]
Linoleoyloxyl	Lipo-ester	/	$C_{18}H_{32}O_2$ (280.2402)	[26]
Oleoyloxyl	Lipo-ester	/	$C_{18}H_{34}O_2$ (282.2559)	[26]
Stearoyloxyl	Lipo-ester	/	$C_{18}H_{36}O_2$ (284.2715)	[26]
Benzoyloxyl	Aromatic ester	$[C_7H_5O]^+$ (105.0335)	$C_7H_6O_2$ (122.0368)	R.S. & [27]
Cinnamoyloxyl	Aromatic ester	$[C_9H_7O]^+$ (131.0491)	$C_9H_8O_2$ (148.0524)	[28]
Anisoyloxyl	Aromatic ester	$[C_8H_7O_2]^+$ (135.0441)	$C_8H_8O_3$ (152.0473)	[28]
Veratroyloxyl	Aromatic ester	$[C_9H_9O_3]^+$ (165.0546)	$C_9H_{10}O_4$ (182.0579)	[28]

Tips:
"/": No corresponding diagnostic fragment ions or neutral losses.
"R.S.": These diagnostic ions or neutral losses were selected based on high-fragment IM-MS spectra of their reference standards (R.S.).
" [24−28]": These diagnostic ions or neutral losses were selected based on previously reported literatures.

identification criteria, polymeric diterpene alkaloids were not taken into consideration in this study. Based on the conventional structures of all potential skeletons (Fig. 5-A) and ester-substituents (Fig. 5-B) for diterpene alkaloids, the compounds with DBEs less than six were not considered and manually excluded. For most of aminol diterpene alkaloids, their DBEs were not more than eight except for some compounds with special unsaturated substructures (e.g., songoramine, a napelline type diterpene alkaloid with DBE at nine, has two different unsaturated substructures: one O-containing ring and one carbonyl group). For common ester diterpene alkaloids, the ester-groups would provide extra unsaturation degrees on their structures, leading to the DBEs not less than seven according to the skeleton. However, the diagnostic fragmentation behaviors for identification of these diterpene alkaloids were cleavages of ester-bonds, which exhibited as neutral losses of intact acids or characteristic acyl ions. Thus, the compounds with DBE ≥10 but no ester-cleavage behaviors in the high-fragment spectra were temporarily assigned as non-monomeric diterpene alkaloids, which not discussed in this work. Table 2 listed all types of potential structural types for diterpene alkaloids with various DBEs. After this step, 215 precursor ions were retained whereas other 1430 ions (including ions with improper formulas, unsatisfactory DBEs or MS/MS spectra not conformed to diterpene alkaloid fragmentation rules) were

temporarily excluded as non-diterpene alkaloids. These survived 215 compounds were characterized by comparing with previous literatures and analyzing their calculated formulas (with mass errors not exceeded ±5 ppm), DBEs, diagnostic ions, and characteristic neutral losses [31−40].

Interestingly, eight diterpene alkaloids (Compounds 55, 91, 128, 173, 187, 195, 196 and 201) with five potential new esterification types (glycosic, senecioic, crotonic, p-coumaric and azelaic esters) were firstly detected in FZ during interpreting the product ions and fragmentation pathways of detected precursor ions (Fig. S2). For instance, compound 55 presented precursor ions at m/z 600.3382 (Formula: $C_{30}H_{49}NO_{11}$, DBE: 7) in the low-fragment spectra with location (RT, DT) at (19.375 min, 49.082 ms). The high-fragment MS/MS spectra exhibited special fragment ions at m/z 438.2843 and 420.2742, corresponding to consecutive neutral losses of glycosyl moiety ($C_6H_{10}O_5$, 162 Da) and H_2O (18 Da). Besides, m/z 582.3273 and 58.0654 represented neutral loss of H_2O and residue ion of $[C_3H_8N]^+$. Based on the formula and fragment ions, compound 55 was tentatively assigned as 14-O-glycosylneoline, which belonged to unusual glycosylated diterpene alkaloids. Compound 91 (RT 30.566 min, DT 48.515 ms) generated protonated ion at m/z 582.3273 (Formula: $C_{30}H_{49}NO_{11}$, DBE: 8) and product ion at m/z 83.0491 $[C_5H_7O]^+$, corresponding to a tigloyl group in its chemical structure. The product ions at m/z 550.2992, 532.2904, 500.2641, and
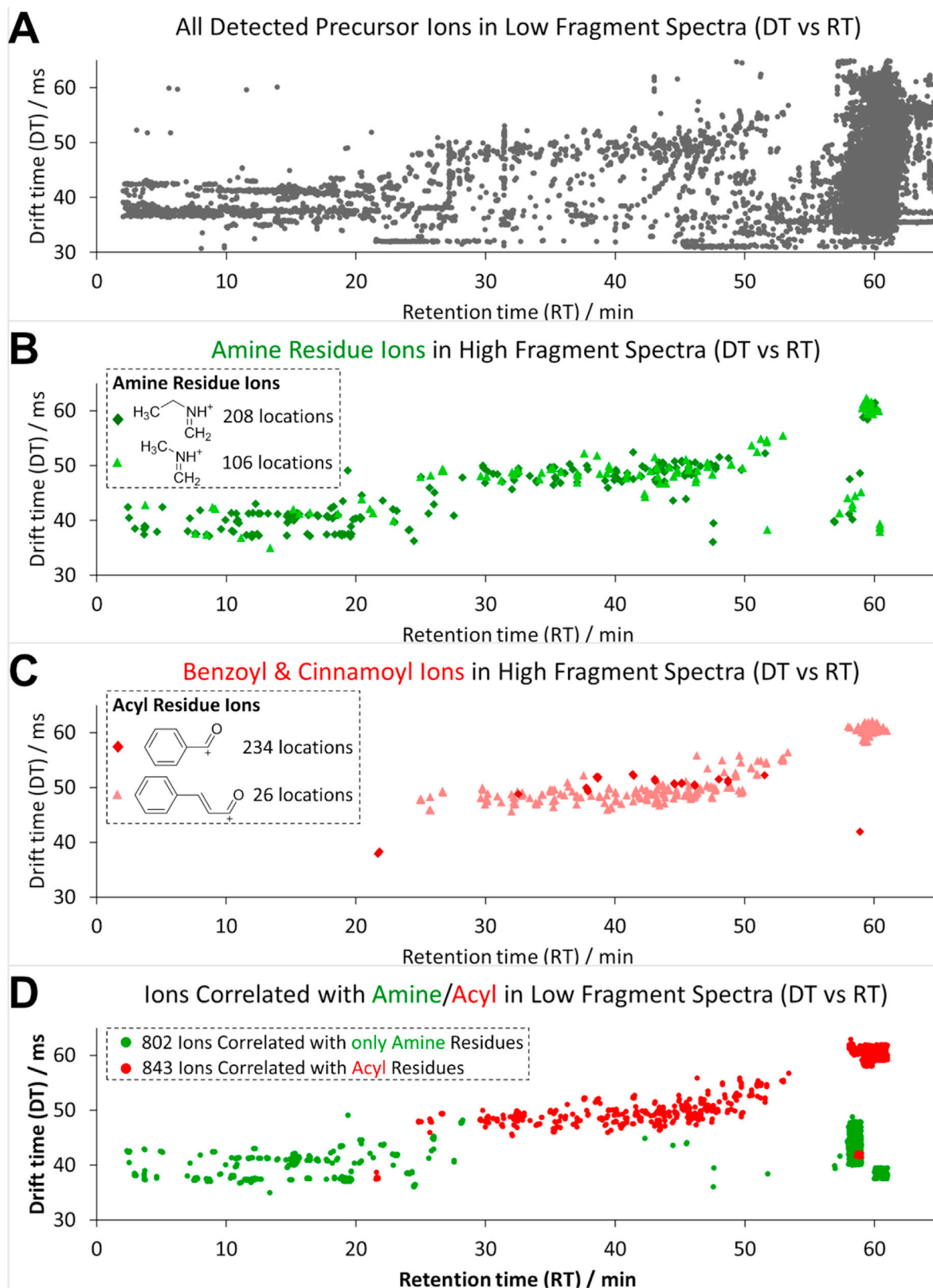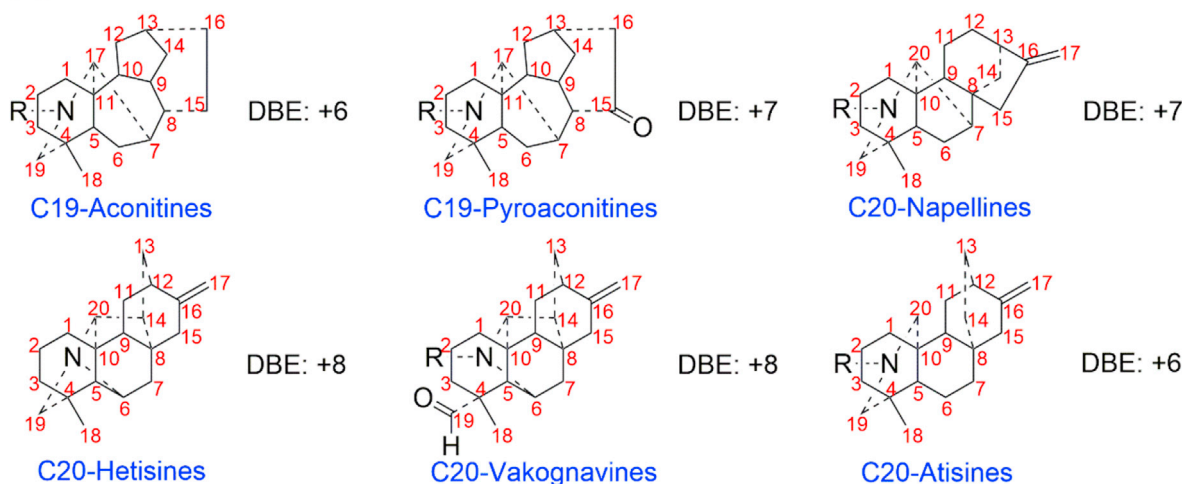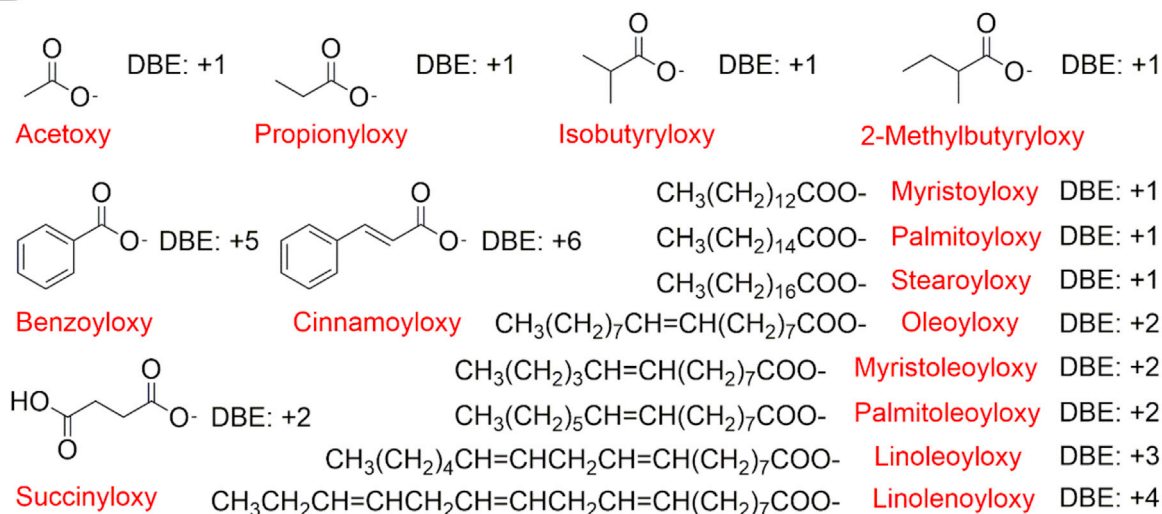
Fig. 4. 2D-distribution (drift times vs retention times) for rapid location of diterpene alkaloids in FZ: All detected precursor ions in low-fragment IM-MS frames (A); Diagnostic amine residue ions in high-fragment IM-MS frames (B); Diagnostic acyl ions in high-fragment IM-MS frames (C); and Extracted precursor ions in low-fragment IM-MS frames correlated with diagnostic fragment ions (D).

A Detected Chemical Skeletons

DBE: +6
C19-Aconitines

DBE: +7
C19-Pyroaconitines

DBE: +7
C20-Napellines

DBE: +8
C20-Hetisines

DBE: +8
C20-Vakognavines

DBE: +6
C20-Atisines

B Detected Common Ester Substituents

DBE: +1
Acetoxy

DBE: +1
Propionyloxy

DBE: +1
Isobutyryloxy

DBE: +1
2-Methylbutyryloxy

DBE: +5
Benzoyloxy

DBE: +6
Cinnamoyloxy

$CH_3(CH_2)_{12}COO-$ Myristoyloxy DBE: +1
$CH_3(CH_2)_{14}COO-$ Palmitoyloxy DBE: +1
$CH_3(CH_2)_{16}COO-$ Stearoyloxy DBE: +1
$CH_3(CH_2)_7CH=CH(CH_2)_7COO-$ Oleoyloxy DBE: +2
$CH_3(CH_2)_3CH=CH(CH_2)_7COO-$ Myristoleoyloxy DBE: +2
$CH_3(CH_2)_5CH=CH(CH_2)_7COO-$ Palmitoleoyloxy DBE: +2
$CH_3(CH_2)_4CH=CHCH_2CH=CH(CH_2)_7COO-$ Linoleoyloxy DBE: +3
$CH_3CH_2CH=CHCH_2CH=CHCH_2CH=CH(CH_2)_7COO-$ Linolenoyloxy DBE: +4

DBE: +2
Succinyloxy

C Detected Potential New Ester Substituents

DBE: +1
Glycosyloxy

DBE: +6
p-Coumaroyloxy

DBE: +2
Crotonoyloxy

DBE: +2
Tigloyloxy
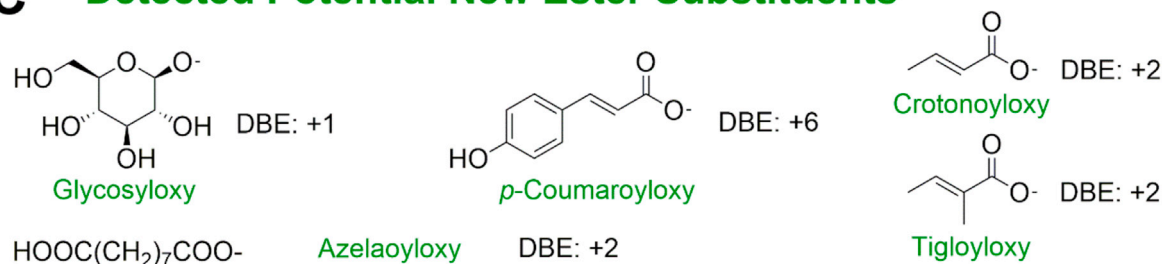
$HOOC(CH_2)_7COO-$ Azelaoyloxy DBE: +2

Fig. 5. Chemical structures and double bond equivalents (DBEs) of all detected substructures for diterpene alkaloids in FZ: Chemical skeletons (A), Common ester substituents (B), and Potential new ester substituents (C).

58.0655 represented fragment ions of $[M + H−C_2H_4O_2]^+$, $[M + H−C_2H_4O_2−H_2O]^+$, $[M + H−C_2H_4O_2−H_2O−C_2H_4O_2]^+$ and $[C_3H_8N]^+$. According to the information mentioned above, it was temporarily annotated as 14-O-tigloylaconine.

Compound **128** (RT 40.512 min, DT 47.009 ms) generated $[M+H]^+$ ion at m/z 536.2631 (Formula: $C_{31}H_{37}NO_7$, DBE: 14) in low-fragment spectra, as well as ions at m/z 450.2263 and 328.1879 in high-fragment spectra, corresponding to consecutively

Table 2. Potential structural types for diterpene alkaloids with various double bond equivalents (DBEs).

DBEs	Potential structural types for diterpene alkaloids
≤5	Considered as non-diterpene alkaloids in this study
6	I. Aminol diterpene alkaloids: C19-aconitines or C20-atisines
7	I. Aminol diterpene alkaloids: C19-pyroaconitines, C20-napellines, or C20-atisines with unsaturated groups
	II. Ester diterpene alkaloids: C19-aconitines or C20-atisines
8	I. Aminol diterpene alkaloids: C20-hetisines, C20-vakognavines, or C20-napellines with unsaturated groups
	II. Ester diterpene alkaloids: C19-aconitines, C19-pyroaconitines, C20-atisines, or C20-napellines
9	I. Partial aminol diterpene alkaloids: C20-napellines with two unsaturated groups
	II. Ester diterpene alkaloids: C19-aconitines, C19-pyroaconitines, C20-atisines, C20-napellines, C20-hetisines, or C20-vakognavines
≥10	I. Considered as ester diterpene alkaloids in this study: C19-aconitines, C19-pyroaconitines, C20-atisines, C20-napellines, C20-hetisines, or C20-vakognavines

Tips: Polymeric diterpene alkaloids were not considered in this study.

neutral losses of intact crotonic acid ($C_4H_6O_2$, 86 Da) and benzoic acid ($C_7H_6O_2$, 122 Da). Additionally, the diagnostic ions at m/z 105.0338 $[C_7H_5O]^+$, 69.0335 $[C_4H_5O]^+$, and 44.0506 $[C_2H_6N]^+$ further suggested the existence of benzoyl, crotonoyl, and N-methyl substructures. Therefore, it was tentatively assigned as 1-Hydroxy-3-crotonyloxy-4-hydroxymethyl-14-benzoyloxy-15-oxo-N-methylaconitane. Compound **173** (RT 46.327 min, DT 55.862 ms, Formula: $C_{40}H_{49}NO_{12}$, DBE: 17) was ambiguously identified as 8-O-p-coumaroyl-14-O-benzoylmesaconine with neutral loss of p-coumaric acid ($C_9H_8O_3$, 164 Da, m/z 736.3324 → m/z 572.2831) as well as diagnostic benzoyl residue ion at m/z 105.0334 $[C_7H_5O]^+$. Moreover, a series of C19 diterpene alkaloids with azelaoyl groups were also detected, which might be generated by degradation of conventional unsaturated long-chain-lipo ester diterpene alkaloids. Compounds **187**, **195**, **196** and **201** presented molecular ions at m/z 760.3902, 774.4046, 744.3959 and 758.4098, respectively. Their calculated formulas possessed same DBEs at 13. Additionally, neutral losses of intact azelaic acid ($C_9H_{16}O_4$, 188 Da) and diagnostic benzoyl ions (m/z 105.03) were observed in all high-fragment IM-MS frames of these four compounds. Based on the formulas and other fragment ions, compounds **187**, **195**, **196** and **201** were tentatively annotated as 8-O-azelaoyl-14-O-benzoylmesaconine, 8-O-azelaoyl-14-O-benzoylaconine, 8-O-azelaoyl-14-O-benzoylhypaconine, and 3-Deoxy-8-O-azelaoyl-14-O-benzoylaconine, respectively.

3.5. Supplementary identification of diterpene alkaloids without selected amine or acyl diagnostic fragment ions

Unfortunately, a fraction of diterpene alkaloids without amine and aromatic ester groups listed in Table 2 were also reported in FZ [24,31–33,39]. For examples, hetisine (C20 hetisine-type alkaloid) [24], carmichaeline B (C20 vakognavine-type alkaloid) [31], and azitine (C20 atisine-type alkaloid) [32] neither have N-methyl/N-ethyl substructures nor possess aromatic acyl groups in their chemical structures. These diterpene alkaloids could not generate the corresponding diagnostic fragment ions, which might be mistaken excluded with the screening step of diagnostic ion guided 2D-locating. In the high-fragment IM-MS frames of these diterpene alkaloids, the ester-cleavage behaviors were exhibited as various neutral losses of intact acids, such as acetic acid ($C_2H_4O_2$, 60 Da), propionic acid ($C_3H_6O_2$, 74 Da), isobutyric acid ($C_4H_8O_2$, 88 Da), and 2-methylbutyric acid ($C_5H_{10}O_2$, 102 Da). For example, carmichaeline B (compound **129**, RT 40.598 min, DT 43.760 ms), a previously reported vakognavine-type diterpene alkaloid [31], generated protonated ion at m/z 500.3010 (Formula: $C_{29}H_{41}NO_6$, DBE: 10) in the low-fragment IM-MS frame. Fragment ions in its high-fragment IM-MS frame at 426.2638, 398.2688, 324.1948 and 296.2014 were characterized as $[M + H-C_3H_6O_2]^+$, $[M + H-C_3H_6O_2-CO]^+$, $[M + H-C_3H_6O_2-C_5H_{10}O_2]^+$ and $[M + H-C_3H_6O_2-CO-C_5H_{10}O_2]^+$, suggesting the propionyloxy, 2-methylbutyryloxy and carbonyl groups in its chemical structure. Compound **154** (RT 44.376 min, DT 44.341 ms) presented precursor ion at m/z 514.3165 (Formula: $C_{30}H_{43}NO_6$, DBE: 10) and similar fragment ions as carmichaeline B at m/z 426.2642 $[M + H-C_4H_8O_2]^+$, 398.2660 $[M + H-C_4H_8O_2-CO]^+$, 324.1933 $[M + H-C_4H_8O_2-C_5H_{10}O_2]^+$ and 296.1987 $[M + H-C_4H_8O_2-CO-C_5H_{10}O_2]^+$. Therefore, compound **154** were tentatively annotated as 2-isobutyryloxy-11-hydroxy-13-(2-methylbutyryloxy)-N-methyl-N,19-secohetisan-19-al, an analogue of carmichaeline B with one unit of isobutyryl at 2-OH rather than propionyl. To further complete the identification of diterpene alkaloids in FZ, 21 compounds were

characterized and supplemented, including 9 heti-sines (Compounds **33**, **37**, **64**, **69**, **72**, **73**, **75**, **82** and **193**), 10 vakognavines (Compounds **78**, **88**, **115**, **129**, **139**, **152**, **154**, **172**, **177** and **188**) and 2 atisines (Compounds **169** and **176**).

3.6. LC-IM-MS distribution analysis of all diterpene alkaloids detected in FZ

Combining the 215 compounds obtained by diagnostic ion guided 2D-locating in section 3.4 and 21 compounds supplemented in section 3.5, 236 compounds were detected and characterized as diterpene alkaloids in FZ, including 61 aminol alkaloids (42 C19-types and 19 C20-types), 144 non-lipo-ester alkaloids (113 C19-types and 31 C20-types), and 31 lipo-ester alkaloids (31 C19-types). The detailed information of characterized diterpene alkaloids in FZ were listed in Table S1. Their chemical structures were shown in Fig. S3, Fig. S4, and Fig. S5. The 2D-distribution (DT vs RT and DT vs m/z) of these diterpene alkaloids was exhibited in Fig. 6.

Initially, the 2D-distribution of diterpene alka-loids' DTs and RTs were discussed, which reflected the correlation between the polarities and spatial sizes. It is well-known that ester alkaloids usually possessed larger sizes and weaker polarities than aminol alkaloids due to the existence of ester-groups, which exhibited as larger DTs and RTs, respectively. Therefore, the lowly toxic aminol diterpene alkaloids usually distributed at lower left area of the rectangular plane coordinate system with DT as y-axis and RT as x-axis (brown and blue dots), whereas highly toxic ester-type diterpene alkaloids located at upper right area (pink, purple, and yellow dots). As shown in Fig. 6-A, most of the C20-diter-pene alkaloid datapoints (blue and purple dots) were located at the below of C19-diterpene alkaloid datapoints (brown, pink, and yellow dots). It was indicated that the spatial structures of C20-diter-pene alkaloids were relatively smaller than C19 within similar esterification degrees. These phe-nomena might be caused by the following reasons: (i) the C20-skeletons possessed less hydroxylation sites than C19-skeletons in general, and (ii) the C20-diterpene alkaloids usually had double-bonds in their structures. These structural characteristics might shrink the spatial sizes of C20-diterpene al-kaloids. Another type of interested compounds were the special C19 lipo-ester alkaloids (yellow dots). These diterpene alkaloids possessed extremely larger RTs and DTs than conventional non-lipo-ester alkaloids. It might because the existence of long-chain-lipo groups substantially reduced the

polarities and significantly extended the spatial shapes.

The trendlines of diterpene alkaloids' DTs with m/z revealed the relationship between their spatial sizes and molecular weights. As shown in Fig. 6-B, the DTs of holistic characterized diterpene alkaloids exhibited a good linear correlation with the coeffi-cient (R) at 0.987952. The respective linear correla-tion for individual diterpene alkaloid structure types of C19 aminol, C19 non-lipo-ester, C19 lipo-ester, C20 aminol, and C20 ester diterpene alkaloids were further investigated and discussed. For C19 types, the DTs of aminol alkaloids presented good linear correlation with $R = 0.988088$ (Fig. 6-C). However, the correlation coefficients (R) became lower for C19 ester alkaloids (Fig. 6-D & E), which might due to the esterification on C19-skeletons impacted the extending direction of their spatial structures. Large ester-groups in the structures could theoretically make obvious influences on the extending di-rections. The C19 lipo-ester alkaloids possessed the lowest correlation coefficient ($R = 0.884730$) comparing with other types owing to the existence of long-chain-lipo ester-groups on their structures. For C20 types, the detected aminol alkaloids possessed various types of skeletons, which might lead to the lower correlation coefficient (R) at 0.928873 (Fig. 6-F). Nevertheless, the C20 ester al-kaloids showed higher correlation coefficient (R) at 0.986968 (Fig. 6-G). These phenomena might be interpreted by the following two reasons. On one hand, most of the detected ester C20 diterpene alkaloid shared the similar skeletons, such as heti-sines and vakognavines. On the other hand, the substituents usually connected at the similar sites on their chemical skeletons.

3.7. Performances of LC-IM 2D-separation on multiple components

Based on the previous reported, the IM possessed certain superiorities on separation of stereoisomers, isobaric compounds, or multiple co-eluted compo-nents, which benefit the discoveries and identifica-tion of more trace components in complex herbal medicines [41−43]. There were several groups of diterpene alkaloid stereoisomers were characterized in FZ. For instance, compounds **142**, **171**, **174**, and **181** shared same formulas as $C_{33}H_{45}NO_9$ but different DTs at 51.503 ms, 48.866 ms, 49.127 ms, and 48.424 ms, respectively. The compounds **142** possessed obviously larger DT, which could be theoretically separated with other three by IM. However, these compounds could also be separated at LC-dimension (RTs at 43.071 min, 46.175 min,
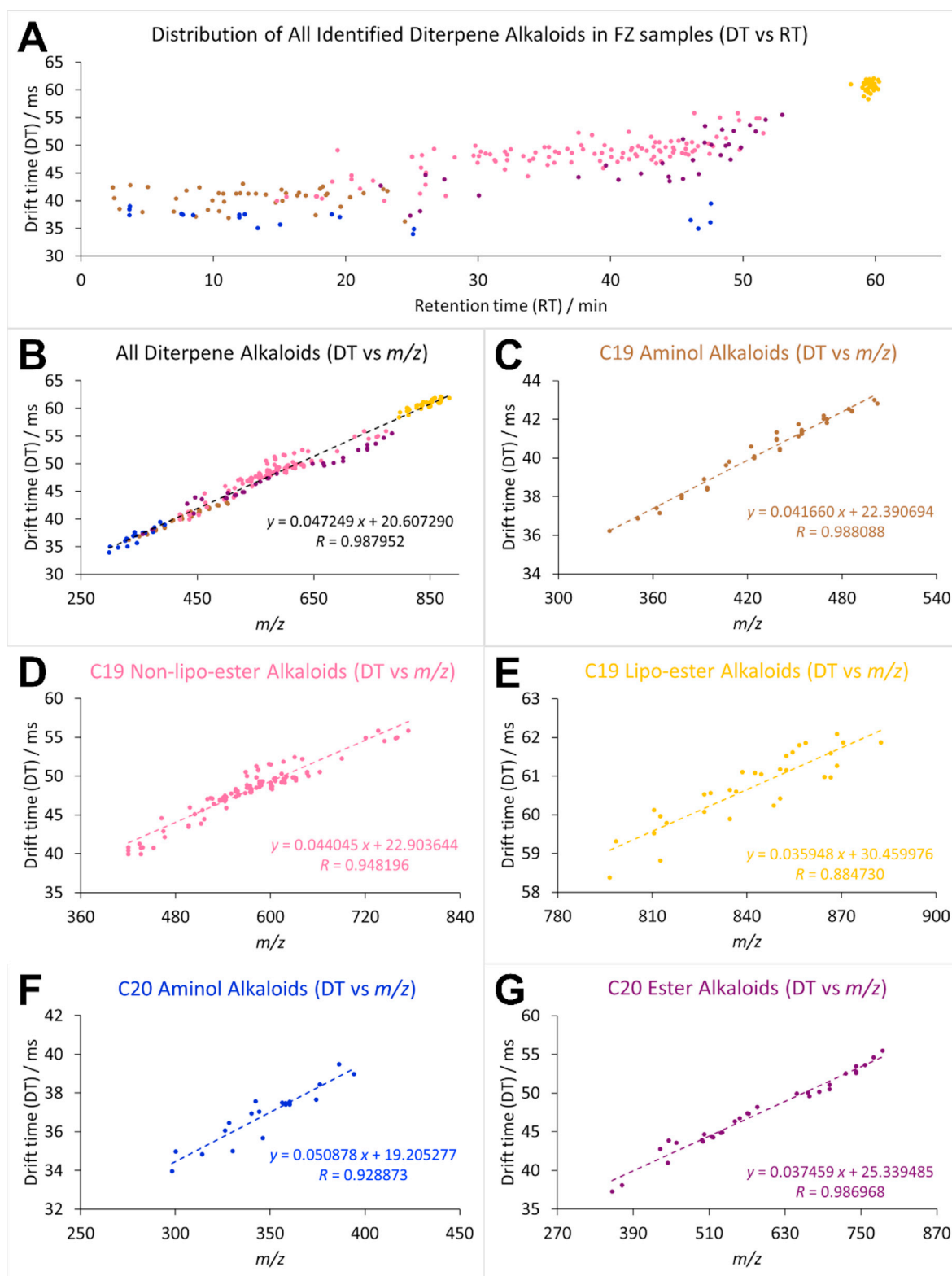
Fig. 6. 2D-distribution of LC-IM separation (drift times vs retention times) for all diterpene alkaloids (**A**) and trendline analysis (drift times vs m/z) for all diterpene alkaloids (**B**), C19 aminol alkaloids (**C**, brown dots), C19 non-lipo-ester alkaloids (**D**, pink dots), C19 lipo-ester alkaloids (**E**, yellow dots), C20 aminol alkaloids (**F**, blue dots), and C20 ester alkaloids (**G**, purple dots) in FZ.
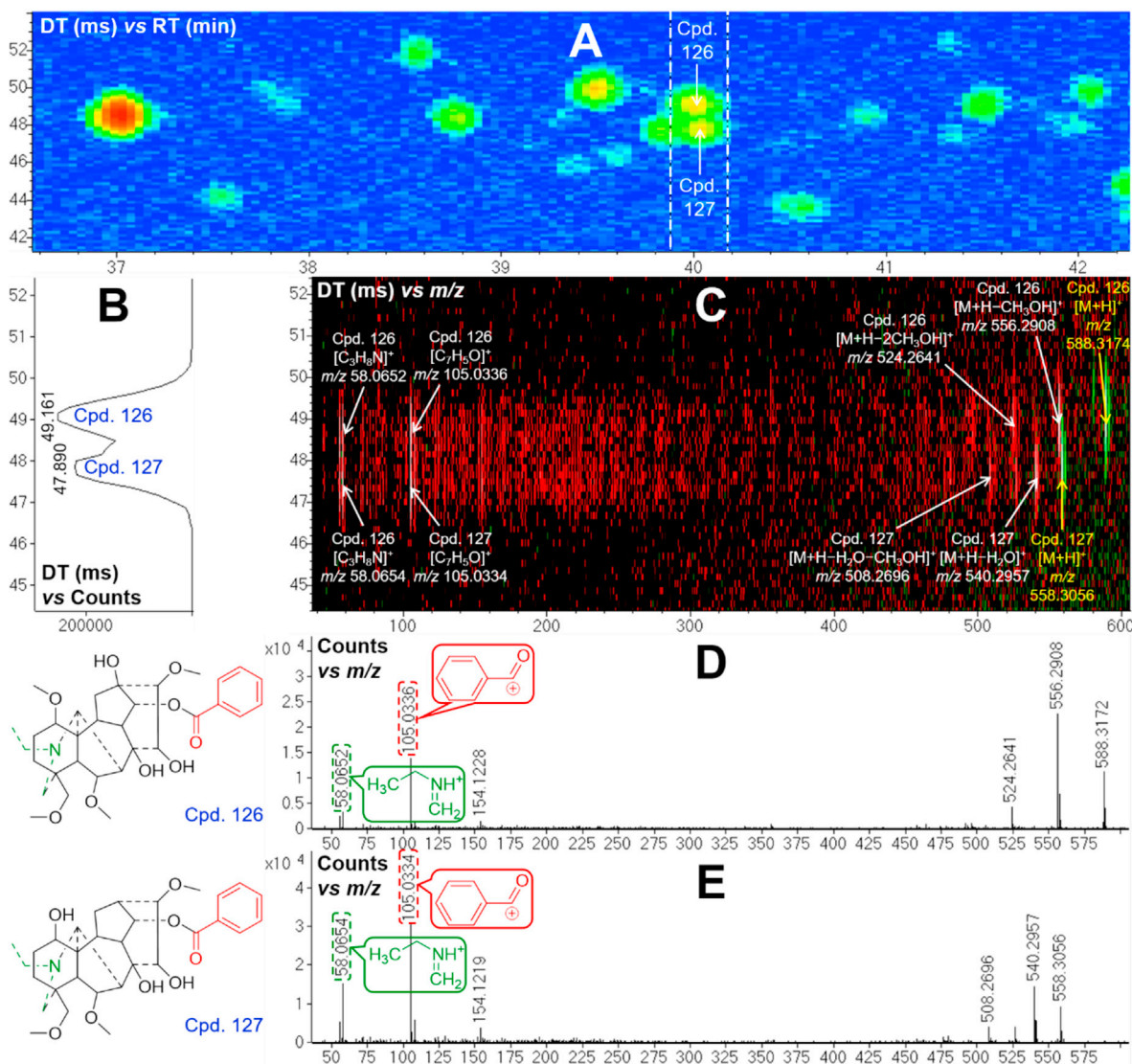
Fig. 7. LC-IM-QTOF MS separation of co-eluted compounds 126 and 127 in FZ: A. LC-IM heatmap (DT vs RT); B. Low-fragment drift spectrum (counts vs DT); C. Overlay low-fragment (green datapoints) and high-fragment (red datapoints) IM-MS frames (DT vs m/z); D. High-fragment IM-MS spectra for compound 126 at DT 49.161 ms (counts vs m/z); E. High-fragment IM-MS spectra for compound 127 at DT 47.890 ms (counts vs m/z).

46.357 min, and 47.483 min for compounds **142**, **171**, **174**, and **181**, respectively), which hidden the role of IM separation. Fortunately, the superiorities of IM were highlighted for separation of LC co-eluted components in this study. For example, LC co-eluted compounds **126** and **127** (RTs at 40.044 min and 40.065 min, Fig. 7-A) presented diverse DTs at 49.161 ms and 47.890 ms (Fig. 7-B), which were separated by IM. More importantly, their fragment ions were located at their respective DTs according to the basis of post-IM fragmentation (Fig. 7-C). By selecting the different DT ranges, the mixed ions were de-convoluted and fragment MS spectra with less interference were obtained for each co-eluted component (Fig. 7-D & E), which benefit the

identification of multiple compounds under DIA modes. Without IM-based separation and deconvolution, the mis-annotation of compounds in complex matrix was more easily to happen.

4. Discussion

Through the operation of the alternating frames-DIA method on LC-IM-MS, a 2D-locating strategy based on RTs and DTs of diagnostic fragment ions was developed to reveal the profiles and distribution of chemical analogues with toxicities in potentially toxic herbal materials in this study. This strategy exhibited the combined advantages of 2D-separation, after-IM collision induced dissociation,

and high MS/MS coverage of DIA, which might be beneficial for detecting more components, rapid matching the precursor/product ions, and obtaining more MS/MS information for chemical profiling of complex matrix. More than 200 diterpene alkaloids including eight compounds with five potentially new esterification types were detected and characterized in FZ with the application of developed strategy. These results revealed a comprehensive profile and distribution regularities of diterpene alkaloids with diverse levels of toxicities correlated to their chemical structure types in FZ, which could be rapidly distinguished based on their 2D-locations of RTs and DTs. In a word, this research provide an innovative idea for characterization of small molecular analogues in complex matrix using LC-IM-MS. To some extent, it could extended the application to preliminary assess the risk of potentially toxic herbal medicines by profiling their chemical basis, which could benefit to prevent the accidental poisoning and investigate the poison cases.

Conflict of interest

The authors declared that there were no conflicts of interest.

Acknowledgements

References

[1] Ben-Arye E, Samuels N, Goldstein LH, Mutafoglu K, Omran S, Schiff E, et al. Potential risks associated with traditional herbal medicine use in cancer care: a study of Middle Eastern oncology health care professionals. Cancer 2016;122(4):598−610.

[2] Xiong AZ, Shao YL, Fang LX, Yang X, Zhang SC, Zheng J, et al. Comparative analysis of toxic components in different medicinal parts of Gynura japonica and its toxicity assessment on mice. Phytomedicine 2019;54:77−88.

[3] Singhuber J, Zhu M, Prinz S, Kopp B. Aconitum in Traditional Chinese Medicine-A valuable drug or an unpredictable risk. J Enthopharmacol 2009;126(1):18−30.

[4] Utelli AB, Roy BA, Baltisberger M. Molecular and morphological analyses of European Aconitum species (Ranunculaceae). Plant Systemat Evol 2000;224(3−4):195−212.

[5] Moritz F, Compagnon P, Kaliszczak IG, Kaliszczak Y, Caliskan V, Girault C. Severe acute poisoning with home-made Aconitum napellus capsules: toxicokinetic and clinical data. Clin Toxicol 2005;43(7):873−6.

[6] Wang FP, Chen QH, Liu XY. Diterpenoid alkaloids. Nat Prod Rep 2010;27(4):529−70.

[7] Feng L, Liu WK, Deng L, Tian JX, Tong XL. Clinical efficacy of Aconitum-containing traditional Chinese medicine for diabetic peripheral neuropathic pain. Am J Chin Med 2014; 42(1):109−17.

[8] Kiss T, Borcsa B, Orvos P, Talosi L, Hohmann J, Csupor D. Diterpene lipo-alkaloids with selective activities on cardiac K$^+$ channels. Planta Med 2017;83(17):1321−8.

[9] Nesterova YV, Povetieva TN, Suslov NI, Zyuz'kov GN, Aksinenko SG, Pushkarskii SV, et al. Anti-inflammatory activity of diterpene alkaloids from Aconitum baikalense. Bull Exp Biol Med 2014;156(5):665−8.

[10] Nie JH, Wang F, Ji TF, Zhao J, Zhao FC. Assessment of in vitro cardiotoxicity of extract fractions and diterpene alkaloids from Aconitum leucostomum Worosch: a short communication. J Pharmaceut Biomed Anal 2017;137:84−9.

[11] Wang XJ, Wang HY, Zhang AH, Lu X, Sun H, Dong H, et al. Metabolomics study on the toxicity of Aconite root and its processed products using ultraperformance liquid-chromatography/electrospray-ionization synapt high-definition mass spectrometry coupled with pattern recognition approach and ingenuity pathways analysis. J Proteome Res 2012;11(2):1284−301.

[12] Bonanno G, Ippolito M, Moscarelli A, Misseri G, Caradonna R, Accurso G, et al. Accidental poisoning with Aconitum: case report and review of the literature. Clin Case Rep 2020;8(4):696−8.

[13] Wood C, Coulson J, Thompson J, Bonner S. An intentional aconite overdose: a case report. J Crit Care Med 2020;6(2): 124−9.

[14] Bello-Ramirez AM, Nava-Ocampo AA. A QSAR analysis of toxicity of Aconitum alkaloids. Fund Clin Pharmacol 2004; 18(6):699−704.

[15] Li TF, Gong N, Wang YX. Ester hydrolysis differentially reduces aconitine-induced anti-hypersensitivity and acute neurotoxicity: involvement of spinal microglial dynorphin expression and implications for Aconitum processing. Front Pharmacol 2016;7:367.

[16] Zhang N, Song YL, Song QQ, Shi SP, Zhang Q, Zhao YF, et al. Qualitative and quantitative assessments of Aconiti Lateralis Radix Praeparata using high-performance liquid chromatography coupled with diode array detection and hybrid ion trap-time-of-flight mass spectrometry. J Chromatogr Sci 2016;54(6):888−901.

[17] Kind T, Tsugawa H, Cajka T, Ma Y, Lai ZJ, Mehta SS, et al. Identification of small molecules using accurate mass MS/MS search. Mass Spectrom Rev 2018;37(4):513−32.

[18] Ten-Domenech I, Martinez-Sena T, Moreno-Torres M, Sanjuan-Herraez JD, Castell JV, Parra-Llorca A, et al. Comparing targeted vs. untargeted MS2 data-dependent acquisition for peak annotation in LC-MS metabolomics. Metabolites 2020;10(4):126.

[19] Chien HJ, Wang CS, Chen YH, Toh JT, Zheng YF, Hong XG, et al. Rapid determination of isoflavones and other bioactive compounds in soybean using SWATH-MS. Anal Chim Acta 2020;1103:122−33.

[20] Samanipour S, Reid MJ, Baek K, Thomas KV. Combining a deconvolution and a universal library search algorithm for the nontarget analysis of data-independent acquisition mode liquid chromatography-high-resolution mass spectrometry results. Environ Sci Technol 2018;52(8):4694−701.

[21] Wu Q, Wang JY, Han DQ, Yao ZP. Recent advances in differentiation of isomers by ion mobility mass spectrometry. Trac Trends Anal Chem 2020;124:115801.

[22] Baker ES, Tang KQ, Danielson WF, Prior DC, Smith RD. Simultaneous fragmentation of multiple ions using IMS drift time dependent collision energies. J Am Soc Mass Spectrom 2008;19(3):411−9.

[23] Mairinger T, Kurulugama R, Causon TJ, Stafford G, Fjeldsted J, Hann S. Rapid screening methods for yeast sub-metabolome analysis with a high-resolution ion mobility quadrupole time-of-flight mass spectrometer. Rapid Commun Mass Spectrom 2019;33(S2):66−74.

[24] Hu R, Zhao J, Qi LW, Li P, Jing SL, Li HJ. Structural characterization and identification of C19- and C20-diterpenoid alkaloids in roots of Aconitum carmichaeli by rapid-resolution liquid chromatography coupled with time-of-flight mass

spectrometry. Rapid Commun Mass Spectrom 2009;23: 1619−35.

[25] Wang FP, Chen DL, Deng HY, Chen QH, Liu XY, Jian XX. Further revisions on the diterpenoid alkaloids reported in a JNP paper (2012,75,1145-1159). Tetrahedron 2014;70(15): 2582−90.

[26] Csupor D, Wenzig EM, Zupko I, Wolhart K, Hohmann J, Bauer R. Qualitative and quantitative analysis of aconitine-type and lipo-alkaloids of Aconitum carmichaeli roots. J Chromatogr A 2009;1216(11):2079−86.

[27] Gao W, Liu XG, Liu L, Li P, Yang H. Targeted profiling and relative quantification of benzoyl diterpene alkaloids in Aconitum roots by using LC-MS/MS with precursor ion scan. J Separ Sci 2018;41(18):3515−26.

[28] Shim SH, Kim JS, Kang SS. Norditerpenoid alkaloids from the processed tubers of Aconitum carmichaeli. Chem Pharm Bull 2003;51(8):999−1002.

[29] Jaiswal YN, Liang ZT, Ho A, Wong LL, Yong P, Chen HB, et al. Distribution of toxic alkaloids in tissues from three herbal medicine Aconitum species using laser micro-dissection, UHPLC-QTOF MS and LC-MS/MS techniques. Phytochemistry 2014;107:155−74.

[30] Yang MB, Ji XY, Zhong Zuo. Relationships between the toxicities of radix aconiti lateralis preparata (Fuzi) and the toxicokinetics of its main diester-diterpenoid alkaloids. Toxins 2018;10:391.

[31] Jiang BY, Lin S, Zhu CG, Wang SJ, Wang YN, Chen MH, et al. Diterpenoid alkaloids from the lateral root of Aconitum carmichaelii. J Nat Prod 2012;75(6):1145−59.

[32] Shen Y, Liang WJ, Shi YN, Kennelly EJ, Zhao DK. Structural diversity, bioactivities, and biosynthesis of natural diterpene alkaloids. Nat Prod Rep 2020;37(6):763−96.

[33] Liang Y, Wu JL, Li X, Guo MQ, Leung ELH, Zhou H, et al. Anti-cancer and anti-inflammatory new vakognavine-type alkaloid from the roots of Aconitum carmichaelii. Tetrahe-dron Lett 2016;57(52):5881−4.

[34] Qin XD, Yang S, Zhao Y, Gao Y, Ren FC, Zhang DY, et al. Five new C-19-diterpenoid alkaloids from Aconitum carmi-chaeli. Phytochem Lett 2015;13:390−3.

[35] Chan TYK. Aconite poisoning. Clin Toxicol 2009;47(4):279−85.

[36] Takayama H, Wu FE, Eda H, Oda K, Aimi N, Sakai SI. Five new napelline-type diterpene alkaloids from Aconitum liangshanium. Chem Pharm Bull 1991;39(6):1644−6.

[37] Liu XX, Jian XX, Cai XF, Chao RB, Chen QH, Chen DL, et al. Cardioactive C19-diterpenoid alkaloids from the lateral roots of Aconitum carmichaeli "Fu Zi". Chem Pharm Bull 2012; 60(1):144−9.

[38] Murayama M, Mori T, Bando H, Amiya T. Studies on the constituents of Aconitum species. IX. The pharmacological properties of pyro-type aconitine alkaloids, components of processed aconite powder 'Kako-bushi-matsu': analgesic, antiinflammatory and acute toxic activities. J Ethnopharmcol 1991;35(2):159−64.

[39] Zhou GH, Tang LY, Zhou XD, Wang T, Kou ZZ, Wang ZJ. A review on phytochemistry and pharmacological activities of the processed lateral root of Aconitum carmichaelii Debeaux. J Ethnopharmcol 2015;160:173−93.

[40] Zheng JF, Chen L, Huang S, Shan LH, Gao F, Zhou XL. Diterpenoid alkaloids from two Aconitum species with antifeedant activity against Spodoptera exigua. J Nat Prod 2017;80(12):3137−43.

[41] Rister AL, Dodds ED. Ion mobility spectrometry and tandem mass spectrometry analysis of estradiol glucuronide isomers. J Am Soc Mass Spectrom 2019;30(10):2037−40.

[42] Rashid AM, Saalbach G, Bornemann S. Discrimination of large maltooligosaccharides from isobaric dextran and pul-lulan using ion mobility mass spectrometry. Rapid Commun Mass Spectrom 2014;28(2):191−9.

[43] Clayton R, Kendrick J, Holdsworth C, McKenzie D, Weston D, Tomczyk N, et al. Characterisation of co-eluting isomeric metabolites using an ion mobility enabled QTof mass spec-trometer. Drug Metabol Pharmacokinet 2017;32(1):S27−8.